2020 IEEE International Conference on Robotics and Automation (ICRA)
31 May - 31 August, 2020. Paris, France

Grasp Control for Enhancing Dexterity of Parallel Grippers*

Marco Costanzo, Giuseppe De Maria, Gaetano Lettera and Ciro Natale

Abstract— **A robust grasp controller for both slipping avoidance and controlled sliding is proposed based on force/tactile feedback only. The model-based algorithm exploits a modified LuGre friction model to consider rotational frictional sliding motions. The modification relies on the Limit Surface concept where a novel computationally efficient method is introduced to compute in real-time the minimum grasping force to balance tangential and torsional loads. The two control modalities are considered by the robot motion planning algorithm that automatically generates robot motions and gripper commands to solve complex manipulation tasks in a material handling application.**

I. INTRODUCTION

Safe handling of objects with a robotic gripper requires to properly grasp the object to avoid slippage in presence of external disturbances and avoid object damage at the same time. Moreover, as a number of manipulation tasks can require additional dexterity to the gripper, this can be achieved by grippers with several degrees of freedom or by exploiting the so-called extrinsic dexterity [1] while using simpler devices, like parallel jaw grippers. Possessing both manipulation abilities by the same gripping device requires special mechanical solutions like [2] or sophisticated grasp control algorithms [3]. A typical way to improve dexterity of a pinch grasp is to allow rotation of the grasped object about the grasping axis, a maneuver called pivoting. Pivoting can be usefully exploited not only in object manipulation by robotic hands [4] but also in whole-body manipulation [5]. [4] presents a planning algorithm to solve the 3D any-pose-reorienting problem where the pivoting is made possible by a custom gripper that allows both a firm grasp and a pivoting motion of the object but using a special mechanism and a supporting table.

Differently, in our paper [6] we already demonstrated how a parallel gripper equipped with force/tactile sensors can be suitably controlled to achieve both slipping avoidance and controlled sliding by acting on the grasp force. The original model-based algorithm for slipping avoidance computed the grasp force on the basis of the Limit Surface (LS) theory [7]. To improve its robustness against time-varying external disturbances and model uncertainties, a heuristic algorithm exploited the residual of a Kalman filter to increase the grasp force only when necessary. The method worked well with slowly-varying disturbances only, since rapidly changing tangential loads generated residuals even without true slipping motions, due to the dynamics of the Kalman filter itself. Here a different dynamic model is set up to explicitly consider the nonlinear dynamics of the contact and, in turn, to design a nonlinear observer to estimate the relative velocity between the object and the fingers that physically describes the slipping motion. The model consists in the extension of the LuGre friction model [8] to the case of roto-translational sliding based on the use of the LS concept. A new computationally efficient method, based on universal approximators, to numerically compute the LS is also introduced. The control algorithm is described in detail to allow any reader to reproduce it, but no mathematical details are presented, e.g., observability analysis of the nonlinear dynamic model, proof of the closed-loop stability of the control system, even though they are available. This because we want to focus this conference paper on the presentation of the possibilities offered by the in-hand manipulation actions, allowed by the proposed grasp controller, by making them available to the motion planning level. We experimentally demonstrate that a number of complex manipulation tasks, unsolvable with a fixed grasp, are solvable without any re-grasping while using a standard constraint-based motion planner with minimal modifications.

Basically, a virtual rotational joint is added to the kinematic chain along the grasping axis of the gripper that is activated only when a solution with a firm grasp is not found. If a solution exists with the use of the virtual joint, the planner sends a request to the low-level grasp controller to activate the controlled sliding modality only in the motion segments requiring the object or gripper pivoting motions.

II. GRASP CONTROL

Each force/tactile sensor can provide both the measurement of the full 6D contact wrench (composed by a force vector $\boldsymbol{f}_i^{s_i}$ and a moment vector $\boldsymbol{\tau}_i^{s_i}$) $\boldsymbol{h}_i^{s_i}{}^T = (\boldsymbol{f}_i^{s_i}{}^T \ \boldsymbol{\tau}_i^{s_i}{}^T)$ expressed in the sensor frame Σ_{s_i} and the location of the center of pressure on the contact area $\boldsymbol{p}_i^{s_i}$, $i = 1, 2$. Therefore, the external wrench $\boldsymbol{h}_E$ acting on the grasped object can be computed through the grasp matrix $\boldsymbol{W}$ [9], i.e.,

$$\boldsymbol{h}_E^g = \boldsymbol{W} \begin{bmatrix} \boldsymbol{h}_1^g \\ \boldsymbol{h}_2^g \end{bmatrix} \triangleq \boldsymbol{W}\boldsymbol{h}^g. \tag{1}$$

referring the vectors to the grasp frame Σ_g selected as shown in Fig. 1 and, according to the virtual stick concept [10], it is $\boldsymbol{W} = \begin{bmatrix} \boldsymbol{I}_6 & \boldsymbol{I}_6 \end{bmatrix}$. Dually, the internal wrench $\boldsymbol{h}_I$, i.e., that not causing any motion of the object but necessary to generate enough friction forces on the contact areas to hold the object,

*This work was supported by the European Commission within the H2020 REFILLS project ID n. 731590.

The authors are with Dipartimento di Ingegneria, Università degli Studi della Campania "L. Vanvitelli", Via Roma 29, 81031 Aversa, Italy ciro.natale@unicampania.it

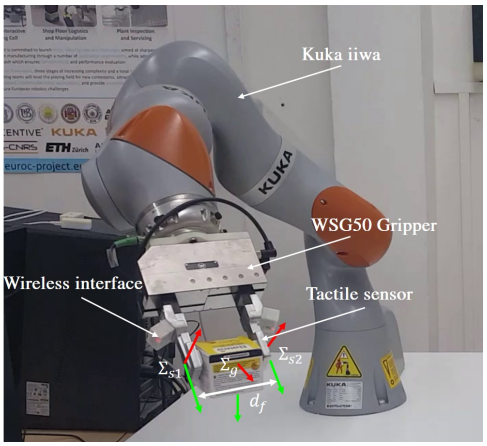

Fig. 1. Gripper used for in-hand manipulation experiments equipped with two force/tactile sensors. Definition of sensor and grasp frames (colors of xyz axes follow the RGB convention commonly used in 3D drawings).

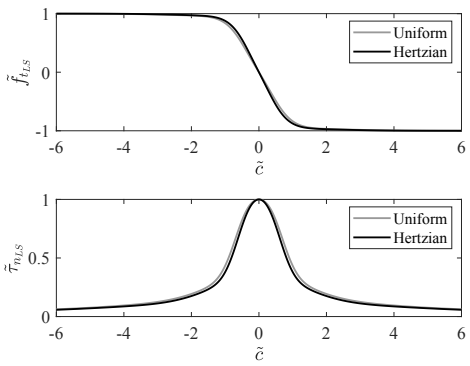

Fig. 2. Typical graphs (uniform and Hertzian pressure distributions) of $\tilde{f}_{t_{LS}}$ and $\tilde{\tau}_{n_{LS}}$ as functions of $\tilde{c}$.

can be obtained as [9]

$$\boldsymbol{h}_I^g = \boldsymbol{V}^\dagger \boldsymbol{h}^g \triangleq \begin{bmatrix} 1/2\boldsymbol{I}_6 & -1/2\boldsymbol{I}_6 \end{bmatrix} \boldsymbol{h}^g, \tag{2}$$

where $\boldsymbol{V}$ is a matrix spanning the null space of $\boldsymbol{W}$. Assuming that the manipulated object has flat rigid surfaces parallel to each other and normal to the z axis of the grasp frame, then, the internal wrench has only one non null component, i.e., the z component, that we call grasping force f_n. By choosing the grasp frame with the y axis aligned with the direction of the tangential force, the external wrench has only two non null components, i.e., the y component of the force that we call tangential force f_t and the z component of the moment that we call torsional moment τ_n.

A low-level linear force control loop commands the velocity of the gripper fingers to ensure that the grasp force follows a given reference. This reference is the so-called grasp force that is computed by the slipping avoidance or controlled sliding algorithms presented in Section II-C and Section II-D, respectively.

A. Virtual Limit Surface

Under the assumptions stated above, the instantaneous rotational motion about the Center of Rotation (CoR) of the manipulated object can be described by a twist vector

$$\boldsymbol{t} = \begin{bmatrix} v_x & v_y & \omega_z \end{bmatrix}^T, \tag{3}$$

where v_x and v_y are the components of the linear velocity and ω_z is the component of the angular velocity. Hence, as shown in [11], the CoR has position

$$\boldsymbol{p}_{\mathrm{CoR}} = \begin{bmatrix} -v_y/\omega_z & v_x/\omega_z & 0 \end{bmatrix}^T, \tag{4}$$

that is orthogonal to $\boldsymbol{t}$.

By kinetostatic duality, the external wrench acting on the object can be represented by the three-dimensional wrench

$$\boldsymbol{w} = \begin{bmatrix} 0 & f_t & \tau_n \end{bmatrix}^T. \tag{5}$$

To characterize the relation between the external wrench and the net friction wrench applied by the soft pad of all fingers to the object, we introduce the concept of *virtual Limit Surface* (LS). It is defined in the wrench plane (f_t, τ_n) as the set of points of the maximum net friction wrench $(f_{t_{LS}}, \tau_{n_{LS}})$ that can balance the external wrench. Assuming that both soft pads have the same physical and geometrical characteristics and the contact surfaces with the object are parallel, a unique virtual pressure distribution over a *virtual contact area* can be defined and then use it to compute the virtual LS. According to the LS theory as recalled in [12], under the assumption of axisymmetric pressure distribution, the CoR position is orthogonal to the direction of the tangential force and thus $v_x = 0$. Therefore, the CoR position has components $\begin{bmatrix} c & 0 & 0 \end{bmatrix}^T$, with $c = -v_y/\omega_z$. The points of the LS can be numerically computed once the pressure distribution and the friction coefficient μ are known by integrating the pressure distribution over the contact area as detailed in [12]. It is common in the literature to compute the normalized LS by introducing the normalized CoR position $\tilde{c}$ with respect to the radius of the contact area and the normalized wrench $(\tilde{f}_{t_{LS}}, \tilde{\tau}_{n_{LS}})$ with respect to the maximum values $f_{t_{\max}}$ and $\tau_{n_{\max}}$ that depend on the grasp force as explained in [13]. It can be easily shown that the results of those integrals are functions of $\tilde{c}$ and their graphs are those reported in Fig. 2 for two typical pressure distributions (Hertzian and uniform). It is relevant to highlight that all axisymmetric pressure distributions considered in [13] generate graphs in between the functions above. Therefore, the normalized tangential and torsional loads are functions of $\tilde{c}$ only, but not of the normal force and are only weakly sensitive to the pressure distribution. Hence, they can be computed only once and they can be approximated by resorting to any universal approximator. Taking into account their typical shapes, it is convenient to use a superposition of sigmoidal functions for $\tilde{f}_{t_{LS}}(\tilde{c})$ and of Gaussian functions for $\tilde{\tau}_{n_{LS}}(\tilde{c})$, which are both radial basis functions and thus can be used as universal approximators [14], [15].

B. Relative Velocity Estimation

With the aim of detecting the slippage of the object, a dynamic model of the instantaneous motion of the object

can be used to estimate the angular velocity of the object ω_z, that is not directly measurable with tactile sensors, however it can be observed. The proposed model is a combination of the LuGre friction model [8] extended to the torsional friction based on the virtual LS and the standard Euler equation of the rigid body motion

$$\dot{\zeta} = \omega_z - \frac{\sigma_0}{g(\cdot)}\zeta|\omega_z| \quad (6)$$

$$\dot{\omega}_z = \frac{1}{J}(-\sigma_0\zeta - \sigma_1\omega_z + u), \quad (7)$$

where ζ is the internal state of the LuGre friction model,

$$g(\cdot) = g(f_n, c) = |\tau_{n_{LS}}| + |c f_{t_{LS}}| \quad (8)$$

is the maximum static friction torque that depends on the normal force f_n and on the instantaneous CoR position c; σ_0 is the so-called asperity stiffness, while σ_1 is the viscous friction coefficient, J is the object inertia moment about the CoR and u is the external torque. Computing $g(\cdot)$ in (8) requires computation of $f_{t_{LS}}$ and $\tau_{n_{LS}}$ that can be easily obtained using the static model presented above, according to the following procedure

- Compute the CoR position $\tilde{c}$ according to the algorithm presented in [6].
- Compute $\tilde{f}_{t_{LS}}$ and $\tilde{\tau}_{n_{LS}}$ using the universal approximators.
- Denormalize using $f_{t_{\max}}$ and $\tau_{n_{\max}}$.

It can be shown that the dynamic model (6) and (7) with the output equation

$$y = \sigma_0\zeta + \sigma_1\omega_z. \quad (9)$$

is locally weakly observable and the following nonlinear observer

$$\dot{\widehat{\zeta}} = \widehat{\omega}_z - \frac{\sigma_0}{g(\cdot)}\widehat{\zeta}|\widehat{\omega}_z| \quad (10)$$

$$\dot{\widehat{\omega}}_z = \frac{1+l}{J}\left(-\sigma_0\widehat{\zeta} - \sigma_1\widehat{\omega}_z + y\right), \quad (11)$$

for any positive gain l is such that $\widehat{\omega}_z$ asymptotically converges to ω_z. The formal proof is omitted for brevity and because the paper is more focused on the experimental verification of the proposed approach.

C. Slipping Avoidance

Using this control modality, the grasp force is computed to avoid any object motion inside the gripper. Similarly to the slipping control strategy in [6], the reference f_n of the low-level grasp force controller is computed as the superposition of a static contribution f_{n_s} and a dynamic one f_{n_d}. The first one is sufficient to hold the object only when a static external disturbance is applied to object, namely

$$f_{n_s} = \alpha_s f_{n_{LS}}, \quad (12)$$

where α_s is a safety gain slightly larger than 1 to ensure robustness with respect to the uncertainty affecting the computation of $f_{n_{LS}}$, which is the smallest grasp force necessary to bring the point, corresponding to the measured normalized external wrench $(\tilde{f}_t, \tilde{\tau}_n)$, on the normalized LS that is $(\tilde{f}_{t_{LS}}, \tilde{\tau}_{n_{LS}})$. The computation of $f_{n_{LS}}$ starts from estimating $\tilde{c}$ according to the algorithm in [6], then $(\tilde{f}_{t_{LS}}, \tilde{\tau}_{n_{LS}})$ is computed via the universal approximators. Recalling that $\tilde{f}_t = f_t/f_{t_{\max}}$ and that $f_{t_{\max}} = \mu f_n$ [13], [12], then it is

$$f_{n_{LS}} = \frac{f_t}{\mu\tilde{f}_{t_{LS}}}. \quad (13)$$

Note that $f_{t_{LS}}$ depends on $\tilde{c}$, which depends on both torsional and tangential loads.

The dynamic contribution, aimed at counteracting slipping in presence of time varying external disturbances, is here computed as

$$f_{n_d} = \alpha_d|C_d\widehat{\omega}_z|, \quad (14)$$

where $\alpha_d > 0$ is the dynamic gain and C_d is a linear filter necessary to reduce the effect of high frequency noise on the grasp force and the absolute value is needed to ensure an always squeezing grasping force. Note that the dynamic control action vanishes as soon as no slipping occurs, i.e., $\widehat{\omega}_z = 0$. It can be shown that the closed loop system is stable for a sufficiently high α_d such that $g(\cdot) > u$, in fact in this condition the dynamic system (6) and (7) has always an equilibrium point that can be proved to be stable.

D. Controlled Sliding

This is the second control modality made available to the planner and allows a rotational sliding of the object inside the gripper fingers. This can be achieved by bringing the grasping force from its current value to the lowest value that allows to hold the object without loosing the grasp, i.e., f_t/μ, where f_t is obviously the weight of the object measured by the sensorized fingers. This can be obtained by applying a first order linear filter in the discrete time k to the desired value $f_t(k)/\mu$, i.e.,

$$f_{n_{CS}}(k+1) = (1-\alpha_{CS})f_{n_{CS}}(k) + \alpha_{CS}f_t(k)/\mu \quad (15)$$

where the value α_{CS} sets the time constant of the filter. In this way, if the planner has the need to change the gripper orientation with respect to the object and no external torsional moment is applied to the object (e.g., the object is kept vertically), then the resulting motion is a *gripper pivoting* maneuver and the estimated CoR position is close to zero. If a torsional moment is applied to the object, then the object starts rotating inside the fingers and an *object pivoting* maneuver is executed, correspondingly, the estimated CoR position increases from a value close to zero to infinity (a saturation value larger than the maximum radius of the contact area in the implementation).

III. MANIPULATION PLANNING

The objective of the planning procedure described in Section III-B is to solve pick and place tasks in scenarios similar to those depicted in Fig. 3. With reference to the image on top left, suppose that for some reason the robot had to pick the object with that grasp configuration (e.g., to avoid collisions or to reach the object location inside its workspace) and it has to place it on the lower shelf layer with the same orientation. It is obvious that with a fixed

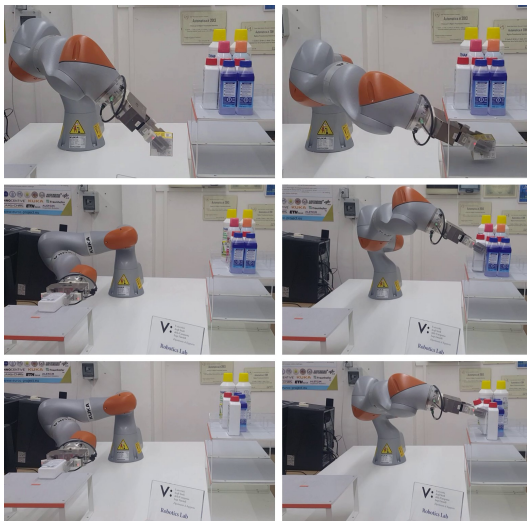

Fig. 3. Three sample scenarios: grasping configurations before (left) and after (right) controlled sliding maneuvers necessary to achieve the goal object pose without collisions.

grasp the planner cannot find any feasible solution due to the collision with the top layer. The availability of changing the gripper orientation without changing object pose (i.e., gripper pivoting) allows the motion planner to find the solution whose final configuration is depicted in the top right picture. Similarly, with reference to the image on middle left, suppose the robot has to pick the bottle placed horizontally on the table and has to place it vertically on the top layer as shown in the middle right image. Again, a fixed grasp solution is unfeasible while an object pivoting maneuver allows the robot to accomplish the task. This is not the only solution. A way to solve the task is to pivot the object on the support table using the algorithm proposed in [4], which could work with our grasp control algorithm, but in our paper a standard motion planner automatically finds the solution simply by using the dexterity offered by the controlled sliding ability. In the last scenario of the bottom pictures, the robot has again to pick the bottle horizontally placed on the table to place it in between two bottles already placed on the same shelf layer on two adjacent facings. To avoid collisions with such objects the bottle has to be placed with a given angle with respect to the vertical direction. Thus, the planner has to find a sequence of robot motions to re-orient the object with respect to the gripper again exploiting the controlled sliding feature of the grasp control.

A. Motion Planner

This section explains how to handle similar scenarios by adding an augmented capability to the motion planner for solving complex tasks, improving its flexibility. The framework adopted for the robot motion planning is MoveIt! [16], which uses the Open Motion Planning Library (OMPL) [17], [18] that implements randomized motion planners. The default Kinematics and Dynamics Library (KDL) [19] kinematic solver has been replaced with Trac-IK [20], which merges a simple extension to KDL's Newton-based convergence algorithm with an efficient Sequential Quadratic Programming (SQP) constrained nonlinear optimization approach.

The task execution is divided into the classical six motion segments of a pick and place task connecting the following target pose sequence: pre-grasp, grasp, pre-grasp, pre-place, place and pre-place. We assume that a grasp planner computed the grasp pose such that a pivoting maneuver is always possible. For each motion segment a planning request is issued by specifying the current robot configuration $\boldsymbol{q}_c$, the object target pose $\boldsymbol{p}_t$, the position and/or orientation constraints $\boldsymbol{c}_t$, the standard kinematic model of the robot r_s and the augmented kinematic model of the robot r_v with the introduction of an additional rotational joint along the grasping axis between the last end effector link and the grasped object, that is made available by the pivoting ability of the grasp controller.

B. Planning with Controlled Sliding

At every planning request, the motion planner tries to plan without using the additional joint (using the standard kinematic model r_s) and only if the request cannot be satisfied, e.g., in presence of collisions, it attempts to find a solution with the virtual joint (using the augmented kinematic model r_v), i.e., executing a pivoting maneuver. The latter solution allows the planner to change the angle between object and gripper in complex scenarios, e.g., when the object has to be inserted in narrow spaces and/or when a specific place angle is required.

The outputs of each planning request are a vector of motion trajectories $\boldsymbol{\mathcal{T}} = (\mathcal{T}_1, \ldots, \mathcal{T}_n)$ and a vector of gripper control modalities $\boldsymbol{m} = (m_1, \ldots, m_n)$, where $m_i = 0$ means that the slipping avoidance control should be active (fixed grasp) and $m_i = 1$ corresponds to the controlled sliding modality. The length $n = 1, 2, 3$ is automatically selected by the planner depending on the scene, as explained hereafter:

- $n = 1$ the standard planning with fixed grasp is successful ($m_1 = 0$);
- $n = 2$ the target pose $\boldsymbol{p}_t$ is such that the object should be placed vertically and a pivoting maneuver is required to achieve it without collisions. The first trajectory $\mathcal{T}_1$ consists in a pivoting ($m_1 = 1$) with a rotation of the gripper with respect to the object to reach the orientation corresponding to the final target pose compatibly with the obstacles; such pose is denoted with $\boldsymbol{p}_p$. To keep fixed the object position and orientation the motion is planned with suitable constraints $\boldsymbol{c}_p$. The second trajectory $\mathcal{T}_2$ moves the gripper to the final pose with a fixed grasp ($m_2 = 0$).
- $n = 3$ the target pose of the object is not vertical but has a certain angle of rotation about the grasping axis. The first trajectory $\mathcal{T}_1$ is a pivoting ($m_1 = 1$) to allow the gripper to rotate with respect to the object in an orientation that allows to reach the target pose $\boldsymbol{p}_t$ compatibly with the obstacles. Hence, the final pose $\boldsymbol{p}_s$ of this trajectory has the current

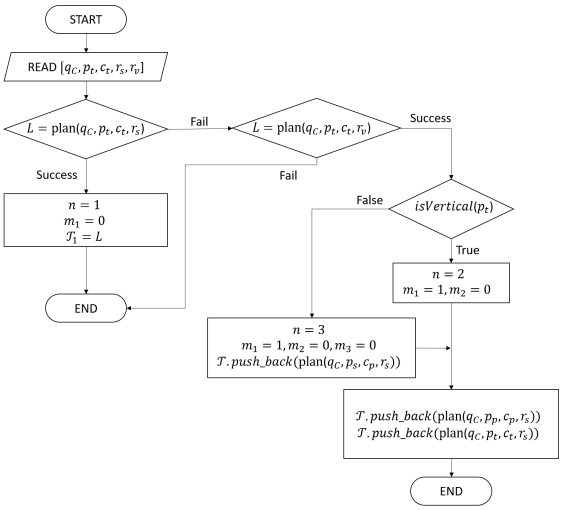

Fig. 4. Flow chart of the planning algorithm: a C++-like expression is used to handle the dynamic length of the vector of planned trajectories $\boldsymbol{\mathcal{T}}$. If planning requests in the cases $n = 2$ and $n = 3$ fail the task is ended.

position of the gripper and an orientation that is the composition of the planned gripper orientation in $\boldsymbol{p}_t$ and the relative orientation between the target pose and the vertical pose. The second trajectory rotates the gripper about the grasping axis with a fixed grasp ($m_2 = 0$) so that the object is brought to an orientation equal to the one in the target pose (hence $\boldsymbol{p}_p$ and $\boldsymbol{p}_t$ have the same orientation). The third trajectory moves the object to the target pose with a fixed grasp ($m_3 = 0$).

Figure 4 shows a flow chart of the planning algorithm.

IV. EXPERIMENTAL RESULTS

The planning and control methods proposed in the paper have been experimentally tested on a Kuka iiwa robot equipped with a Weiss Robotics WSG-50 gripper of Fig. 1. The fingers of the WSG-50 have sensorized with two SUNTouch force/tactile sensors [21], [22] with WiFi 802.11n interface allowing 300 Hz sampling rate. The robot is mounted on a table such that it can reach a first shelf layer to pick the objects (bottom left picture of Fig. 3) to put on a two-layer shelf both on the top (bottom right picture of Fig. 3) and bottom (top right picture of Fig. 3) layers. The planning and control software is implemented under the ROS framework with services, actions and nodes. The control parameters are

$$\alpha_s = 1.1,\ \alpha_d = 13,\ C_d = \frac{s + 5.3}{s + 1.5},\ \alpha_{CS} = 0.004,\ l = 10^3$$

$$\sigma_0 = 40\,\text{Nm/rad},\ \sigma_1 = 0.06\,\text{Nms/rad},\ J = 10^{-3}\,\text{kgm}^2$$

The gain α_s is selected such that the static normal force is 10% higher than that computed with a nominal friction coefficient. The gain α_d is increased until the peak in the dynamic force is high enough to lift the object. The parameter α_{CS} is selected to obtain a time constant of 0.5 with a sampling frequency of 500 Hz. The lag network is tuned to attenuate the measurement noise and the gain l is

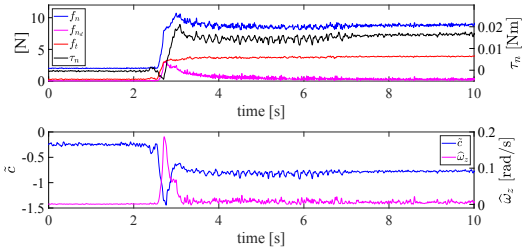

Fig. 5. Preliminary task: quickly lifting an object of unknown weight. Grasp, tangential, dynamic forces and torsional moment (top); normalized CoR on the left axis and estimated relative velocity on the right axis (bottom).

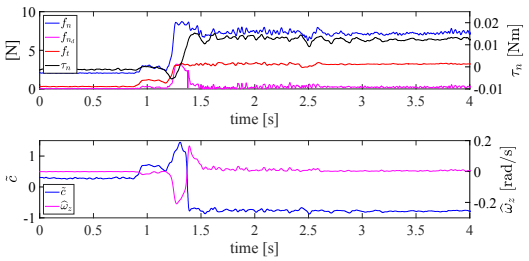

Fig. 6. Preliminary task executed at 100% robot speed override.

increased until y in (9) is tracked by its estimation $\sigma_0\widehat{\zeta}+\sigma_1\widehat{\omega}_z$ without an excessive noise amplification.

A preliminary object lifting task is executed to demonstrate how the grasp control based on the relative velocity observer allows the robot to safely grasp objects of unknown weight (about $380\,\text{g}$) even with quick motions, thus in presence of inertial forces. The object is first grasped far from its CoG with a small force to ensure contact with the sensor and then the slipping avoidance controller is turned on. As soon as the robot starts lifting the object, a relative velocity builds up as it can be recognized in the bottom subplot of Fig. 5. Correspondingly, the dynamic control action computes a force f_{n_d} that has a peak in the initial phase, then it vanishes as soon as the load gets constant. The evidence of no slippage is given by the high value of the torsional moment at steady state that means only a negligible rotation of the object happened (if the object had pivoted, then the gravitational moment would have vanished). At the end of the lifting phase, the tangential load (red line) reaches a value equal to the object weight. The experiment is repeated with a 100% robot speed override and the results are similar, again no object slippage occurs as demonstrated by the results in Fig. 6.

Next, three complete pick and place tasks are executed in the scenarios described in Section III-A, where a solution with a fixed grasp does not exist. However, the planning algorithm proposed in Section III-B is able to solve the task using the controlled sliding manipulation ability made available by the grasp controller in Section II-D:

- Task 1: pick and place of the box as shown in top picture of Fig. 3. The weight is approximately $180\,\text{g}$ and the friction coefficient is about 0.7.

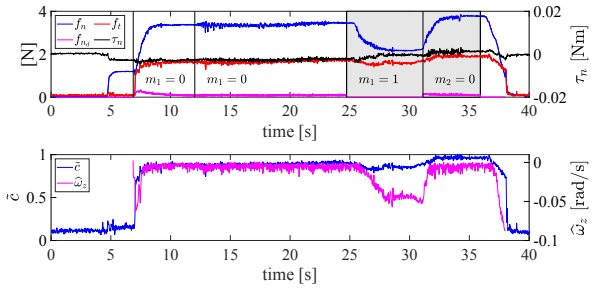

(a) Task 1

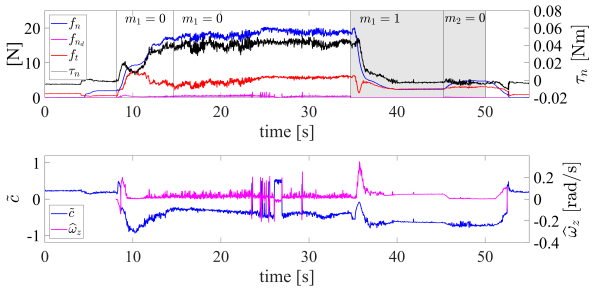

(b) Task 2

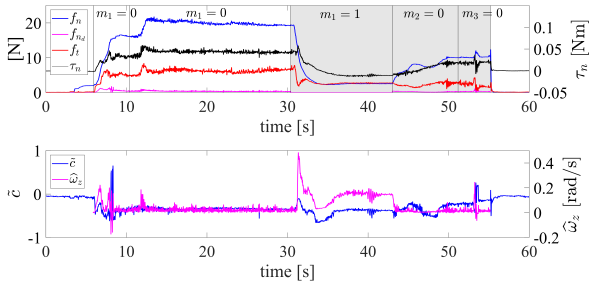

(c) Task 3

Fig. 7. Results of the three manipulation tasks: grasp, tangential, dynamic forces on the left axis and torsional moment on the right axis of top subplots; some planned values of m_i are reported in different planned trajectories identified by vertical bars; the gray-shaded area highlights the motion segment where the planner finds a solution only using the virtual joint (pivoting maneuver), with $n = 2$ for tasks 1 and 2 and $n = 3$ for task 3. The bottom subplots report the estimated normalized position of the CoR $\tilde{c}$ and the estimated relative velocity $\widehat{\omega}_z$.

- Task 2: pick and place of the bottle as shown in middle picture of Fig. 3. The bottle weight is approximately 290 g and the friction coefficient is about 0.9.
- Task 3: pick and place of the bottle as shown in bottom picture of Fig. 3.

Figure 7(a) shows the results of the execution of Task 1. To grasp the object, whose weight is unknown to the robot, a small initial grasp force f_n (blue line in the top subplot) of 1.2 N is applied by the gripper to ensure a contact with the sensors. At about 7 s the robot lifts the object and a peak in the estimated velocity $\widehat{\omega}_z$ rises (magenta line in the bottom subplot) that corresponds to a peak in the dynamic force f_{n_d} (magenta line of the top subplot). The motion is quite slow due to the joint speed limits imposed to the planner for the whole motion, and this explains the low value of the dynamic force. The tangential force f_t (red line) rises up to the weight of the box, while the torsional moment τ_n (black line) is very small during the whole task duration since the origin of the grasp frame is very close to the CoG. In the lifting motion segment from 7 s to 12 s, the planner finds a solution with the standard robot model (see the left branch of the flowchart in Fig. 4). The same happens for the motion segment when the robot moves the grasped box to the pre-place pose (see top left picture in Fig. 3). To reach the target pose shown in the top right picture of Fig. 3, the planner finds a solution by following the right branch of the algorithm flowchart with only two trajectories ($n = 2$) $\mathcal{T}_1$ and $\mathcal{T}_2$. $\mathcal{T}_1$ consists in a rotation of the gripper with a controlled sliding modality ($m_1 = 1$) that allows to keep the orientation of the box fixed. $\mathcal{T}_2$ is a simple motion to the place pose with a fixed grasp ($m_2 = 0$). Note how during the execution of trajectory $\mathcal{T}_1$ the observer estimates a relative velocity during the gripper pivoting but it is not used since the control modality is not slipping avoidance. Moreover, the estimated $\tilde{c}$ is high (close to 1) since the measured torsional moment is very small.

In the execution of Task 2, similar results are shown in Fig. 7(b). But, in the trajectory where the planner finds a solution with the controlled sliding modality active ($m_1 = 1$) the robot does not move as it can be appreciated in the accompanying video but the object rotates in-hand to reach an almost vertical position.

Fig. 7(c) reports the results of the execution of Task 3. Here the target pose is not vertical and thus the planning algorithm follows the corresponding branch of the flowchart. Thus, $n = 3$ and the motion segment from the pre-place pose to the target pose starts with a controlled sliding ($m_1 = 1$) during which the object rotates until the vertical position and the gripper pivots about the grasping axis to reach the orientation of the pose $\boldsymbol{p}_s$ defined in Section III-B. The successive trajectory $\mathcal{T}_2$ rotates the gripper still with a fixed position but with a fixed grasp ($m_2 = 0$) such that the object reaches the orientation of the place pose. The target pose is achieved by executing the last trajectory $\mathcal{T}_3$.

V. CONCLUSIONS

The main result consists in the exploitation of a virtual additional joint at gripper level made available by a suitable low-level grasp control. This additional dexterity is then considered at planning level to solve complex manipulation tasks otherwise unfeasible. Formal proofs of observability of the nonlinear dynamic model and of closed-loop stability have been omitted to focus more on the experimental demonstration of the feasibility of complex manipulation tasks enabled by the combination of the low-level grasp control strategy with a geometric motion planner. Future work will be devoted to presentation of formal results on the closed-loop stability and to the integration of the low-level gripper control with task planners that can autonomously reason on complex scenes to solve the complete shelf refilling task. Further investigation will focus on the generalization to the case of objects with geometry more complex than two flat parallel faces, that requires a more complex definition of the virtual LS used in the grasp controller.

REFERENCES

[1] N. Dafle, A. Rodriguez, R. Paolini, B. Tang, S. Srinivasa, M. Erdmann, M. Mason, I. Lundberg, H. Staab, and T. Fuhlbrigge, "Extrinsic dexterity: In-hand manipulation with external forces," in *2014 IEEE Int. Conference on Robotics and Automation*, Hong Kong, 2014, pp. 1578–1585.

[2] B. Carlisle, K. Goldberg, A. Rao, and J. Wiegley, "A pivoting gripper for feeding industrial parts," in *Proceedings of the 1994 IEEE International Conference on Robotics and Automation*, May 1994, pp. 1650–1655 vol.2.

[3] F. Viña, Y. Karayiannidis, C. Smith, and D. Kragic, "Adaptive control for pivoting with visual and tactile feedback," in *2016 IEEE Int. Conference on Robotics and Automation*, Stockholm, SE, 2016, pp. 399–406.

[4] Y. Hou, Z. Jia, and M. T. Mason, "Fast planning for 3d any-pose-reorienting using pivoting," in *2018 IEEE International Conference on Robotics and Automation (ICRA)*, May 2018, pp. 1631–1638.

[5] E. Yoshida, M. Poirier, J. Laumond, O. Kanoun, F. Lamiraux, R. Alami, and K. Yokoi, "Regrasp planning for pivoting manipulation by a humanoid robot," in *2009 IEEE International Conference on Robotics and Automation*, May 2009, pp. 2467–2472.

[6] M. Costanzo, G. De Maria, and C. Natale, "Slipping control algorithms for object manipulation with sensorized parallel grippers," in *2018 IEEE International Conference on Robotics and Automation*. IEEE, May 2018, pp. 7455–7461.

[7] S. Goyal, A. Ruina, and J. Papadopulous, "Planar sliding with dry friction, part i," *Wear*, vol. 143, pp. 307–330, 1991.

[8] C. Canudas de Wit, H. Olsson, K. J. Aström, and P. Lishinsky, "A new model for control of systems with friction," *IEEE Trans. on Automatic Control*, vol. 40, no. 5, pp. 419–425, 1995.

[9] I. D. Walker, R. A. Freeman, and S. I. Marcus, "Analysis of motion and internal loading of objects grasped by multiple cooperating manipulators," *The International Journal of Robotics Research*, vol. 10, no. 4, pp. 396–409, 1991.

[10] M. Uchiyama and P. Dauchez, "Symmetric kinematic formulation and non-master/slave coordinated control of two-arm robots," *Advanced Robotics*, vol. 7, no. 4, pp. 361–383, 1992.

[11] K. Lynch and F. Park, *Modern Robotics: Mechanics, Planning, and Control*. New York: Cambridge University Press, 2017.

[12] R. D. Howe and M. R. Cutkosky, "Practical force-motion models for sliding manipulation," *The International Journal of Robotics Research*, vol. 15, no. 6, pp. 557–572, 1996.

[13] N. Xydas and I. Kao, "Modelling of contact mechanics and friction limit surfaces for soft fingers in robotics, with experimental results," *The Int. Journ. of Robotics Research*, vol. 18, pp. 941–950, 1999.

[14] J. Moody and C. Darken, "Learning with localized receptive fields," Yale University, Department of Computer Science, Tech. Rep. YALEU/DCS/RR-649, 1988.

[15] K. Hornik, "Approximation capabilities of multilayer feedforward networks," *Neural Networks*, vol. 4, no. 2, pp. 251 – 257, 1991.

[16] I. A. Sucan and S. Chitta, "Moveit!" http://moveit.ros.org, accessed: 2019-08-31.

[17] I. A. Sucan, M. Moll, and L. E. Kavraki, "The Open Motion Planning Library," *IEEE Robotics & Automation Magazine*, vol. 19, no. 4, pp. 72–82, December 2012.

[18] Z. Kingston, M. Moll, and L. E. Kavraki, "Decoupling constraints from sampling-based planners," in *International Symposium of Robotics Research*, Puerto Varas, Chile, 2017.

[19] R. Nilsson, "Inverse kinematics," Master's thesis, Lulea University of Technology, Sweden, 2009.

[20] P. Beeson and B. Ames, "TRAC-IK: An open-source library for improved solving of generic inverse kinematics," in *2015 IEEE-RAS 15th International Conference on Humanoid Robots (Humanoids)*. IEEE, nov 2015, pp. 928–935.

[21] G. De Maria, C. Natale, and S. Pirozzi, "Force/tactile sensor for robotic applications," *Sensors and Actuators A: Physical*, vol. 175, pp. 60 – 72, 2012.

[22] M. Costanzo, G. De Maria, C. Natale, and S. Pirozzi, "Design and calibration of a force/tactile sensor for dexterous manipulation," *Sensors*, vol. 19, no. 4, 2019.